Characterization of Seismicity from Different Glacial Bed Types: Machine Learning Classification of Laboratory Stick-Slip Acoustic Emissions

S. Saltiel[1]†, N. Groebner[2], T. Sawi[1], C. McCarthy[1], B.K. Holtzman[1]

[1] Lamont-Doherty Earth Observatory, The Earth Institute, Columbia University of New York, NY, USA

[2] Strabo Analytics, Inc, New York, NY, USA.

Corresponding author: Seth Saltiel (ssaltiel@unr.edu)

† now at Nevada Seismological Laboratory, University of Nevada, Reno, NV, USA

Key Points:

- Ice slip on frozen till or rock at high velocity produce stick-slip stress-drops with AEs recorded on transducers frozen into the ice
- Supervised learning can predict whether an event waveform originated from frozen till or rock, but spectral features are not predictive
- Feature importance shows that till events are more impulsive, they generally have higher steady-state friction and stress-drops

Abstract

Subglacial seismicity provides the opportunity to monitor inaccessible glacial beds in high resolution. There are different types of glacial beds, which determine the mechanics of slip and, if unstable, characteristics of resulting seismicity. Utilizing a double direct shear apparatus, we found conditions for instability at freezing temperatures and high slip rates for both rock and till beds, although with very different frictional evolution. During stick-slip stress-drops, we recorded acoustic emissions with piezoelectric transducers frozen into the ice. Supervised machine learning can classify recorded waveforms as coming from rock or till, while spectral information is not predictive. The Random Forest Classifier is interpretable, with the prediction based on the first three oscillation peaks. Till events are generally higher stress-drop, with more impulsive first arrivals compared to rock waveforms. These seismic signatures of mechanical slip processes and associated bed conditions can potentially greatly enhance interpretation of subglacial seismic data.

Plain Language Summary

A glacier can lurch forward while slipping on its base, like an earthquake, releasing seismic waves which are monitored from the surface. Just like in a tectonic setting, only certain conditions allow for this type of motion, and aspects of the bed conditions affect the mechanics of slip and resulting waveforms. We replicate realistic glacial bed conditions in the lab of two very different types, soft (sediment) and hard (rock), and measure lurching behavior and resulting waves from each. Using a variety of data science techniques, we decipher subtle differences between the two bed types from ‘remotely-sensed’ waves. This suggests that seismicity can provide important information on glacial bed conditions and how they differ in time and space.

1 Introduction

Future sea-level rise will largely be determined by fast-slipping polar glaciers, known as ice streams [Cuffey & Paterson 2010]. Since motion is mostly concentrated at their beds, conditions in this region have an outsized effect on the entire system’s mass-balance and evolution. Glacial beds are separated, to first order, into hard bedrock or soft sediment (till), and then as either wet (melting temperature) or dry (frozen or drained) [Clarke 2005]. Water and sediment can move and change on much shorter time scales than ice deforms, so the bed is one of the most dynamic parts of the ice sheet system, assumed to be responsible for recent changes in ice flow configurations [Bougamont et al., 2015] and ongoing responses to the changing climate [Parizek et al., 2013].

Although the basal system is difficult to directly access, growing observations of subglacial seismicity offer the opportunity to monitor changes with high temporal and spatial resolution [Aster & Winberry 2017]. Recent studies have used subglacial seismicity observations to infer differences in bed strength [Guerin et al., 2021], failure mechanism [Kufner et al., 2021], fine-scale asperity interactions [Gräff et al., 2021], basal water pressure [Gräff & Walter 2021], as well as local basal shear-stresses and slip-rates [Hudson et al., 2022].

Seismic observations are particularly useful since there are limited glacial bed conditions that have been shown to exhibit the requisite conditions for seismic failure [Iverson 2010, Lipovsky et al., 2019]. Classically, ice deformation, and thus slip due to regelation and viscous creep, is assumed to be rate-strengthening [Schoof 2005]. Till deformation was also first treated as viscous but later shown to be Coulomb plastic, essentially rate-neutral [Iverson 2010, Zoet & Iverson 2020]. But nucleation of seismic instability requires rate-weakening resistance, described by the rate-state stability parameter ($b - a$), which allows acceleration due to feedback with decreasing friction, as has been shown for fault rocks and gouge [Marone 1998]. This situation provides the opportunity for seismic observations to present a strong constraint on the conditions at their epicentral location and origin time, but each potential stick-slip mechanism and resulting seismicity characteristics must be thoroughly understood to determine what recorded seismic events represent.

Laboratory simulations provide the opportunity to directly observe slip behavior under controlled subglacial conditions. To date, seismically required rate-weakening has been reported for debris-laden ice on impermeable rock at sub-freezing temperature and permeable rock at the pressure melting point [Zoet et al., 2013], pure ice on impermeable rock at sub-freezing temperature [McCarthy et al., 2017], and pure ice on till at sub-freezing temperature [Saltiel et al., 2021], with stick-slip stress-drops only reported for debris-laden ice on impermeable rock at sub-freezing temperature [Zoet et al., 2020]. These findings suggest that seismicity is largely associated with dry (frozen or drained) conditions, but experiments have also shown rate-weakening is possible due to cavity formation behind hard bed obstacles [Zoet & Iverson 2016] and pore-pressure feedback from clast ploughing [Thomason & Iverson 2008]. Although each of these mechanisms, and the bed conditions which enable them, show rate-weakening drag, their frictional evolution can differ dramatically. For example, the critical slip distance (D_c) over which friction evolves to a new steady-state after a change in slip rate varies by more than an order of magnitude between rock and till beds under similar conditions in the same apparatus [McCarthy et al., 2017, Saltiel et al., 2021]. These mechanisms' different frictional characteristics and applicable scales likely contribute to aspects of the resulting seismicity, which could further constrain epicentral bed conditions.

We report here, for the first time, experimental stick-slip stress-drops for pure ice on impermeable rock and till at sub-freezing temperatures. In addition, we measured Acoustic Emissions (AEs) from these settings and analyze the measured waveforms using Machine Learning (ML) classification algorithms to find the characteristics associated with each bed type and its resulting mechanics. By improving our understanding of the mechanisms of unstable slip in glacial settings and their expression in seismic emissions, these experiments and analysis techniques provide the opportunity to extract more information of conditions / source mechanics of subglacial or other seismic settings.

2 Experimental Methods and Materials

Experiments were conducted using an ambient pressure, cryogenic temperature, servo-hydraulic biaxial friction apparatus [McCarthy et al., 2016], with modifications to the insulating cryostat and loading procedure to allow measurement of till [Saltiel et al., 2021]. In this double-direct-shear configuration, a central ice block slides against two stationary side blocks, with layers of pre-compacted and frozen till or rock, on opposite sides of the ice, such that applied horizontal load is resolved as normal stress and vertical load as shear stress on the sliding interfaces (Figure 1a). Additional experimental details are described in supporting text S1.

We made three additional modifications to the apparatus from that past study. An additional Linear Variable Inductance Transducer (LVIT) position sensor measures the sample displacement separate from the loading point's preset displacement. This allowed measurement of displacement in each stress-drop 'slip' event as well as how much slip occurs during 'stuck' periods and the timing of both relative to stress-drops (Figure 1c). Here we refer only to mechanical or bulk stress-drops, the stress change during a slip event as measured by our vertical load cell, not to be confused with seismologically derived stress-drops. A rubber gasket material was also inserted into the loading geometry that effectively reduced the stiffness of the apparatus, reaching critical stiffness and allowing stick-slip instability. We estimate the effective apparatus stiffness using the mechanical data's reloading slope between stress-drops, relative to the compression of the loading train including rubber, the load point displacement minus sample displacement (Figure 1c). We estimate the apparatus stiffness after adding the rubber to be ~ 0.1 kPa/µm or ~ 5 x 10^5 N/m, significantly less stiff than was estimated without the rubber ~ 1 kPa/µm [Saltiel et al., 2021]. Additionally, commercial piezoelectric transducers were frozen into the central ice block, facing one of the ice-bed interfaces, to measure AEs. After experimenting with four different types of transducers of varying sizes and frequency sensitivities, we settled on Physical Acoustic's Nano-30™ miniature AE sensor due to its small size and 125-750 kHz response, covering the major frequency content of the events. All AEs analyzed here were recorded with a single Nano-30.

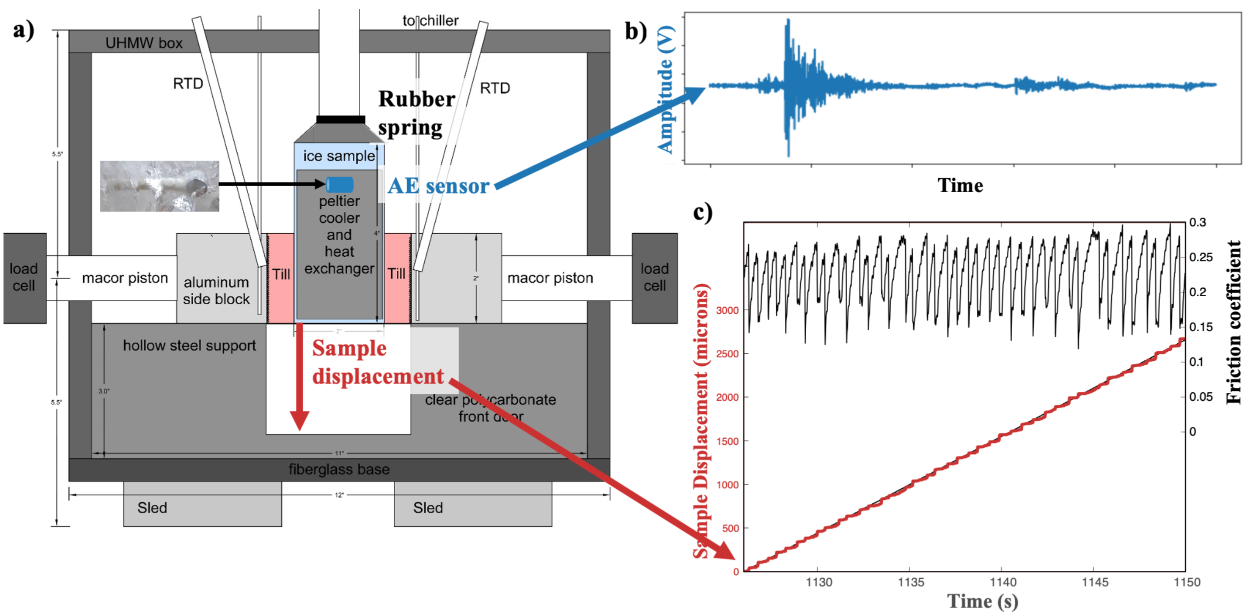

Figure 1: a) Schematic of biaxial cryostat with additions of rubber spring to decrease loading stiffness, AE sensor frozen into central ice bock (pictured within ice in inset on left), and sample displacement measurement, modified from Saltiel et al., [2021]. **b)** An example AE waveform before processing, from a single stress-drop / slip event, and **c)** an example experiment of measured friction drops (in black on top) and stick-slip sample displacement (in red on the bottom) with the steady load point displacement (in black) for reference, due to instability induced by apparatus reaching subcritical stiffness.

AEs were recorded using a preamplifier and TiePie™ HS6 differential digital oscilloscope. To ensure we recorded all relevant spectral content in the waveforms, they were recorded at a very high sample rate of 100 MHz for 2 ms time windows around each triggered event. These oscilloscope settings provided the optimum real-time viewing of triggered waveforms as they were being recorded (Figure 1b), but subsequent analysis showed most of the energy was under 1 MHz, and waveforms were subsequently down sampled to 10 MHz and windowed to 15 µs, lowering file size. Recordings of continuous acoustic signal without applied shear found electrical noise above 3 MHz, so filtering also helped remove persistent noise sources. The oscilloscope was set in rising-limb trigger mode with trigger amplitude set just above the noise level before the deformation program started, such that it did not trigger without an audible stress-drop. Since electrical and other sources of noise can vary, this trigger level was adjusted throughout the experiment to maximize the number of captured events and minimize waveforms of purely noise, but some events were missed, and many events triggered by noise were saved.

3 Data Processing and Machine Learning Analysis

To remove noisy events, non-events triggered by noise, and to normalize the waveform in a way that focuses on the initial wave arrivals, we implemented a data cleaning and normalization approach based on that implemented by Nolte & Pyrak-Nolte [2022], described in supporting text S2.

After removing noisy waveforms, we end up with 2817 total events, including 1547 waveforms from 6 till experiments and 1270 waveforms from 6 rock experiments. With this labeled catalog (Figure 2), we systematically explored the predictive performance of numerous supervised ML algorithms on the waveforms as well as on spectra and spectrograms creating from the waveforms. We found that none of the spectral-based algorithms were substantially more predictive than random (at best ~55%), so here we focus on waveform-based results.

We divide the data into training and test sets based on experiment, i.e., for a given model training run the waveforms from 5 till and 5 rock experiments are used for the training set, and the remaining 1 till and 1 rock experiment are used for testing. By separating training and test sets by experiment, any experiment-dependent features of the waveforms would be irrelevant for classification. As experiments vary in number of events (between 94 – 465), we calculated balanced prediction accuracy for each set of test data. The prediction accuracy is summarized by a 6 till by 6 rock experiments matrix, giving the accuracy for 36 models with each combination used as the testing data (Figure 3).

We focus our analysis on the Random Forest Classifier model [Breiman 2001] applied to processed waveforms, since it obtained some of our highest prediction accuracies (68% mean accuracy), independent of which experiments were used for testing, and it gives the feature importance for interpretability. The feature importance shows the weighting of each waveform sample in making predictions (Figure 4a). The feature importance is key for interpreting how the prediction is made and visually highlighting the subtle differences between different waveform sources.

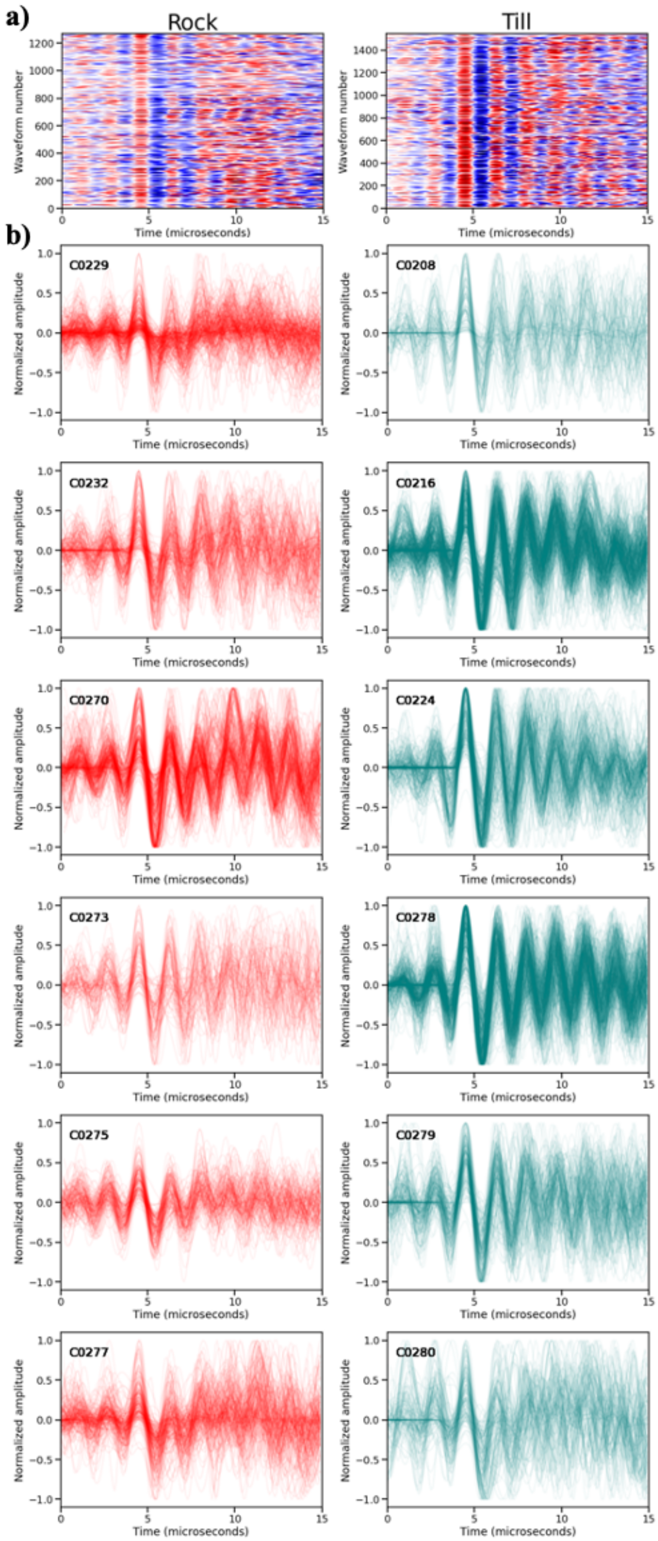

Figure 2: a) Waveforms plotted in chronological order along y-axis, oldest experiments, lower number, on bottom, colored by amplitude and normalized by maximum amplitude (red is positive and blue negative) with rock events plotted on left and till on the right. **b)** Waveforms plotted together for each experiment (labelled on upper left). Rock experiments are plotted in red, while the till events are teal. Each waveform is plotted with a thin, light line, so the dark parts show many waveforms aligned on top of each other, and broader lines show less alignment. Since experiments vary significantly by number of events (94 – 465), that also contributes to the appearance of each experiment plot. Although there are subtle differences, it is not visually clear that the two beds can be deciphered, making it a useful dataset to explore ML-based classification.

4 Results and Discussion

Using a wide range of classification algorithms, we consistently find prediction accuracy above 50%, mostly between 60% and 85%, showing it is possible to tell if waveforms were emitted by till or rock beds. This is not clear by visually examining the waveforms (Figure 2), showing algorithms successfully extract subtle waveform features correspond to the different bed labels. Our preliminary explorations found almost no predictive power in the spectral data, including spectra, spectrograms, and further extracted. In contrast, every method of processing the waveform data and every algorithm we tested, found some overall predictive capability in the waveforms.

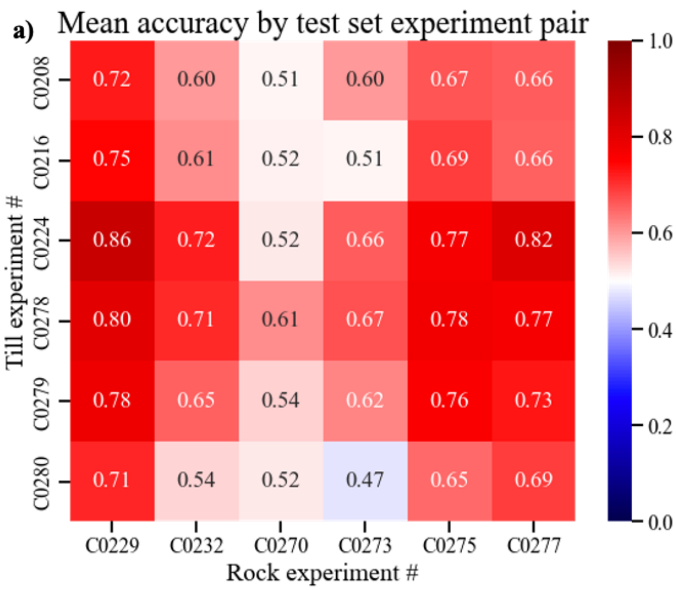

Figure 3: a) Mean prediction accuracy given different sets of rock and till experiments used as testing dataset. In each case, the rest of the experiments were used as training data, producing a model for each combination of testing experiments (6 till and 6 rock experiments make for 36 different train and test datasets, and models). Although some experimental variation is expected, relatively consistent results across testing datasets shows that the overall predictability is not experiment dependent. **b)** Table on right provides the temperature range, number of events, and accuracy for each individual experiment.

b)

Exp. (C0#)	Bed type	Temp (~°C)	# of events	Accu -racy
208	Till	-3	94	67%
216	Till	-3	465	71%
224	Till	-2.5	245	86%
278	Till	-3.4	421	82%
279	Till	-4	181	74%
280	Till	-4	141	63%
229	Rock	-6 => -4	319	82%
232	Rock	-4 => -3	184	51%
270	Rock	-3	296	38%
273	Rock	-3.8	95	42%
275	Rock	-4.3 => -3.9	150	71%
277	Rock	-3.9	226	68%

This prediction accuracy calculates how often the model could correctly classify individual waveforms as coming from till or rock beds, but we envision a tool whereby a collection of seismic events recorded from a given location would be analyzed to determine the probability it came from a till or rock-based glacier. So, the more relevant accuracy is if a single experiment can be accurately predicted to be till or rock, and how many events would be needed to make such a prediction accurate. By this metric, all 6 till experiments would be correctly predicted (with total test accuracies well above 50%), while only 3 rock experiments are robustly predicted as rock. This shows that the model is very sensitive to till features, able to detect them in all the till experiments, but more specific for rock, in that every experiment predicted as rock was correct. Even though the algorithms correct for class imbalances there is a minimum number of events that are needed to give accurate results, which can be analyzed using a receiver operating characteristic (ROC) curves. This minimum catalog size, along with seismicity rates, would set the maximum temporal and spatial resolution of bed identification through this method.

To be able to apply our findings from laboratory AEs to field-scale seismicity, it is vital that we can interpret how the algorithms make their prediction. Although transfer learning methods offer the potential to train with labelled laboratory or modelled datasets and ‘transfer’ the model to more limited field or laboratory data [Wang et al., 2021], clear differences in the spectral content, path effects, and scale of field seismic data make this a daunting task. But by isolating and interpreting the features the algorithms are using to make their successful predictions, we can understand the differences in the waveforms to look for and interpret in field data. The feature importance for all 36 Random Forest Classifier models show similar parts of the waveform are used to make the prediction, focusing on the first three peaks (positive and negative) of the initial wave arrivals (Figure 4a). Plotting all the normalized waveforms (color coded by bed type) on top of each other, we can see that the till (teal) waves tend to have higher amplitude in these first peaks (Figure 4b). Analyzing the mechanical data from 23 till and 22 rock experiments (including other experiments without recorded AEs, in addition to those described above), we find that the stress-drops of stick-slip events on till beds are generally higher (Figure 4c). This difference in stress-drop is consistent with till’s higher healing rates (Figure 4d) and higher average friction (Figure 5), but given the range of values for each and subtlety of waveform differences, ML techniques were needed to quantify how accurately bed-type can be deciphered from waveforms. Along with the fact that till events are generally predicted more accurately, we interpret the algorithm’s attention to initial arrivals as evidence that this till feature is the main identification and the rest are classified as rock.

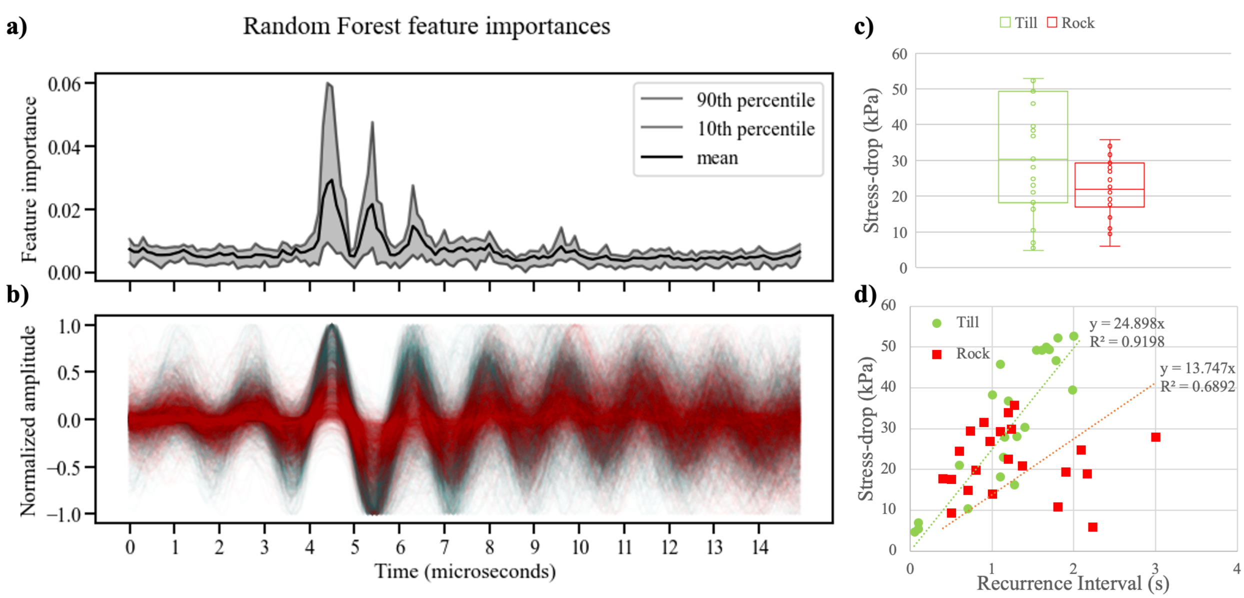

Figure 4: a) Mean feature importance, showing the relevance of each waveform sample to the models’ prediction, with 10th and 90th percentile error bands for all 36 Random Forest Classifier models, and **b)** plot of all rock (red) and till (teal) waveforms. Results highlight the importance of

the initial three wave arrivals in all models. Plotting the superimposed normalized waveforms, shows that the till (teal) events are higher amplitude in these first few oscillations. **c)** Box and whisker plots of largest repeated mechanical stress-drop amplitude from 23 till and 22 rock experiments at similar stress and temperature conditions show till also has higher stress-drops, although with overlap. **d)** Stress-drops vs their recurrence interval for till and rock experiments, the till beds' greater healing (higher slope) contributes to their higher stress-drops.

These experiments also show the temperature dependence of instability, as both rock and till experiments were over a range of temperatures. Although analyzing the temperature dependence of AEs is outside of the scope of this letter, we find stick-slip instability is limited to frozen temperatures (< ~ 0 °C for rock and < ~ -2.5 °C for till beds in Figure 5. Given temperatures are approximate, since they are measured behind the till/rock, there is some lag time before the temperature on the sliding interface reached those recorded. This finding is consistent with that of rate-weakening friction in till beds at ~ -3 °C using the same apparatus [Saltiel et al., 2021]. We estimate the apparatus stiffness with rubber to be ~ 0.1 kPa/μm or ~ 5 x 10^5 N/m, which is the same order of magnitude as the critical stiffness of estimated from velocity-step experiments ~ 0.02 kPa/μm or 1 × 10^5 N/m at similar conditions (see section on critical stiffness in Saltiel et al., [2021]). This factor of five difference is consistent with the error inherit in applying estimations of rate-state friction parameters ($b - a$, D_c) from few experiments, as well as in our rough estimation of apparatus stiffness. Past studies of ice-on-rock friction did not find rate-weakening until lower temperatures, < ~ -18 °C for McCarthy et al., [2017] using this apparatus. In that study, experiments above -18 °C which exhibited slight rate-strengthening were undertaken at less than half the slip rate, which could affect the rate-dependence of friction as well as stability more broadly [Schulson & Fortt 2012]. It is also possible to reach instability at nominally stable conditions given the strong elastic contrast between ice and rock beds [Rice et al., 2001]. This highlights the range of factors that contribute to seismic instability. Further experiments and analysis are needed to fully map subglacial stability.

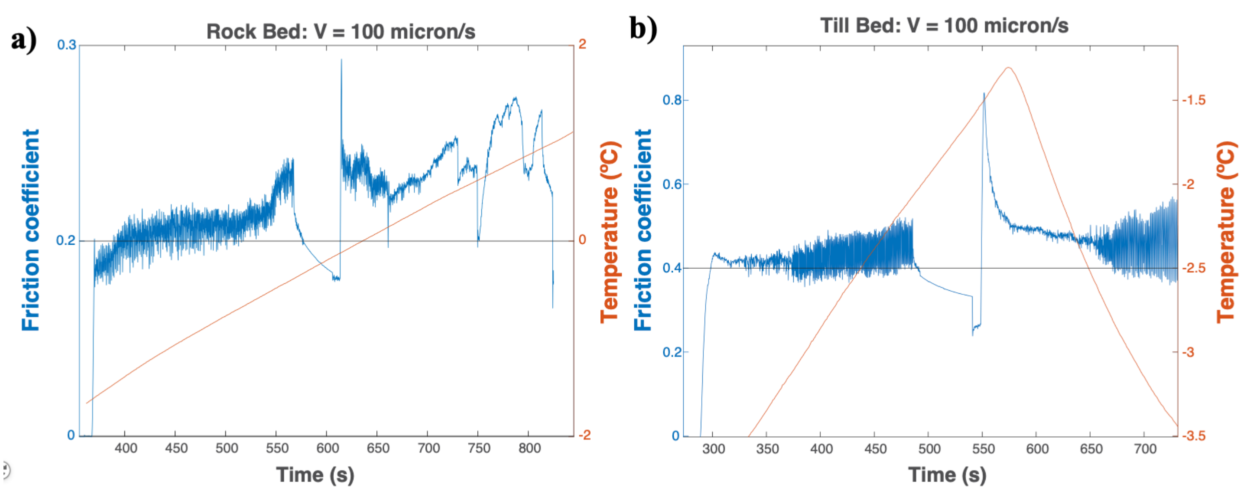

Figure 5: Example experiments of the temperature effect on slip stability for **a)** rock and **b)** till beds. Each experiment shows stress-drops in the beginning of the experiment but, after an experimentally induced hold (described in supporting text S1), with increasing temperature the ice starts to stably slide without sudden drops in friction or audible stick-slips. The transition to stable sliding occurs around ~ 0 °C for the rock experiment. In the till experiment, stability is reached during the hold, but as the temperature is lowered again stress-drops resume after reaching ~ -2.5

°C. Each estimated transition temperature is highlighted with a solid black horizontal line. The till experiment has higher friction and healing rate (as the friction coefficient rose significantly more after hold times of similar duration).

5 Conclusions

This study presents stick-slip stress-drops and resultant AE waveforms for ice on rock and till beds at sub-freezing temperatures, a labeled dataset in which we explore how ML can decipher which bed produced the events. We found that instability, and thus seismicity, only occurs for each bed below a certain temperature (~ 0 °C for rock and ~ -2.5 °C for till), sliding stably as the temperature warms above and stick-slipping again when frozen below that temperature. Although the different bed types exhibit stick-slip behaviors at similar conditions, the mechanics of their drag are very different, demonstrated by friction that evolves over an order of magnitude more distance (D_c), significantly more rate-weakening ($b - a$), higher friction, and healing rates in frozen till compared to rock beds [Saltiel et al., 2021]. The higher healing rates contribute to the generally higher stress-drops (Figure 4d). Resultant emissions have subtle differences, difficult to decipher visually, but which ML-based classification was able to identify; successfully predicting the bed type of a given waveform about 60% to 85% of the time. Given the events from an entire experiment, all 6 till experiments were correctly identified, but only half of the rock experiments were robustly predicted. In contrast, spectral data was not predictive. The Random Forest Classifier was particularly successful and interpretable, since it provides feature importance of each waveform sample, showing the models focus on the first three wave arrivals, where till waveforms are higher amplitude. This is consistent with more impulsive failure, higher stress-drops, friction, and healing.

These findings are counter to our original hypothesis based on the longer frictional evolution distances (D_c) found in velocity-step experiments, which suggest less impulsive, lower frequency emissions. It is possible that different aspects of the frictional mechanics counter each other, for example more healing has been associated with higher frequency emissions in laboratory and natural faults [McLaskey et al., 2012], which could cancel the spectral effect of longer D_c. In a similar way, till experiments' higher D_c and $b - a$ balance each other to produce a critical rheological stiffness of the same order as rock [Saltiel et al., 2021]. In the end, our findings suggest that ML-based classification and correlation studies could find unknown and non-intuitive relationships between seismic emission characteristics and the mechanics / conditions of rupture in subglacial, as well as tectonic, volcanic, induced seismicity settings. Laboratory experiments offer the opportunity to obtain well-controlled, labeled datasets, but results need to interpretable. Although it will be difficult to transfer models trained in the lab directly to field-scale data, the understanding gained can be used to infer characteristics of natural or induced seismic sources.

Acknowledgments, Samples, and Data

S. Saltiel acknowledges the support of the Lamont-Doherty Postdoctoral Fellowship in Earth and Environmental Sciences. This research and S. Saltiel and C. McCarthy were funded by National Science Foundation (NSF)-1854629. Many thanks to T. Mittal for data processing and ML analysis suggestions, J. Tielke and T. Koczynski for laboratory assistance, as well as C. Marone, J. Rivière, and the Penn State Rock and Sediment Mechanics Lab for experimental acoustics advice.

The datasets generated for this study are available on figshare.com at doi: 10.6084/m9.figshare.21257730, and Jupyter notebook for processing data is available at https://github.com/StraboAI/IcesAEs.

References

Aster, R. C., & Winberry, J. P. 2017. Glacial seismology. *Reports on Progress in Physics*, **80**, 126801. doi:10.1088/1361-6633/aa8473

Bougamont, M., Christoffersen, P., Price, S. F., Fricker, H. A., Tulaczyk, S., & Carter, S. P. 2015. Reactivation of Kamb Ice Stream tributaries triggers century-scale reorganization of Siple Coast ice flow in West Antarctica. *Geophysical Research Letters*, **42**(20), 8471-8480.

Breiman, L. 2001. Random Forests. *Machine Learning* **45**, 5–32 doi:10.1023/A:1010933404324

Clarke, G. K. 2005. Subglacial processes. *Annual Review of Earth and Planetary Sciences*, **33**(1), 247-276.

Cole, D. M. 1979. Preparation of polycrystalline ice specimens for laboratory experiments, *Cold Reg. Sci. Technol.*, 1, 153–159, doi: 10.1016/0165-232X(79)90007-7.

Cuffey, K.M. & Paterson, W.S.B., 2010. The Physics of Glaciers, 4th ed, Elsevier

Gräff, D., Köpfli, M., Lipovsky, B. P., Selvadurai, P. A., Farinotti, D., & Walter, F., 2021. Fine structure of microseismic glacial stick-slip. *Geophysical Research Letters*, **48**, e2021GL096043. https://doi. org/10.1029/2021GL096043

Gräff, D., & Walter, F., 2021. Changing friction at the base of an Alpine glacier. *Sci. Rep.* **11**, 10872. https://doi.org/10.1038/s41598-021-90176-9

Guerin, G., Mordret, A., Rivet, D., Lipovsky, B. P., & Minchew, B. M., 2021. Frictional origin of slip events of the Whillans Ice Stream, Antarctica. *Geophysical Research Letters*, **48**(11), e2021GL092950.

Iverson, N.R., 2010. Shear resistance and continuity of subglacial till: hydrology rules. *Journal of Glaciology*, **56** (200) 1104-1114. doi:10.3189/002214311796406220.

Hudson, T., Kufner, S. K., Brisbourne, A., Kendall, M., Smith, A., Alley, R., ... & Murray, T. 2022. Friction and slip measured at the bed of an Antarctic ice stream., Preprint from *Research Square*, DOI: 10.21203/rs.3.rs-1214097/v1

Kufner, S.-K., Brisbourne, A. M., Smith, A. M., Hudson, T. S., Murray, T., Schlegel, R., et al. 2021. Not all icequakes are created equal: Basal icequakes suggest diverse bed deformation mechanisms at Rutford Ice Stream, West Antarctica. *Journal of Geophysical Research: Earth Surface,* 126, e2020JF006001. Doi:10.1029/2020JF006001

Lipovsky, B.P., Meyer, C.R., Zoet, L.K., McCarthy, C., Hansen, D.D., Rempel, A.W. & Gimbert, F., 2019. Glacier sliding, seismicity and sediment entrainment. *Annals of Glaciology*, **60**(79), pp.182-192.

Marone, C., 1998. Laboratory-derived friction laws and their application to seismic faulting, *Ann. Rev. Earth Planet. Sci.*, **26**, 1, 643–696.

McCarthy, C., Savage, H.M., Koczynski, T., & Nielson, M.A., 2016. An apparatus to measure frictional, anelastic, and viscous behavior in ice at temperate and planetary conditions. *Review of Scientific Instruments*, **87**.

McCarthy, C., Savage, H.M., & Nettles, M., 2017. Temperature dependence of ice-on-rock friction at realistic glacier conditions, *Phil. Trans. R. Soc. A*, **375** (2086), 20150348.

McLaskey, G. C., Thomas, A. M., Glaser, S. D., & Nadeau, R. M., 2012. Fault healing promotes high-frequency earthquakes in laboratory experiments and on natural faults. *Nature*, **491**(7422), 101-104.

Nolte, D. D., & Pyrak-Nolte, L. J., 2022. Monitoring fracture saturation with internal seismic sources and twin neural networks. *Journal of Geophysical Research: Solid Earth*, **127**(2), e2021JB023005.

Parizek, B. R., Christianson, K., Anandakrishnan, S., Alley, R. B., Walker, R. T., Edwards, R. A., Wolfe, D. S., Bertini, G. T., Rinehart, S.K., Bindschandler, R. A., & Nowicki, S. M. J., 2013. Dynamic (in) stability of Thwaites Glacier, West Antarctica. *Journal of Geophysical Research: Earth Surface*, **118**(2), 638-655.

Rice, J. R., N. Lapusta, & Ranjith K., 2001. Rate and state dependent friction and the stability of sliding between elastically deformable solids, *J. Mech. Phys. Solids*, **49**, no. 9, 1865–1898.

Saltiel, S., McCarthy, C., Creyts, T. T., & Savage, H. M., 2021. Experimental evidence of velocity-weakening friction during ice slip over frozen till: Implications for basal seismicity in fast moving, soft-bed glaciers and ice streams. *Seismological Research Letters*, **92**(5), 2793-2810.

Schoof, C. 2005. The effect of cavitation on glacier sliding. *Proceedings of the Royal Society A: Mathematical, Physical and Engineering Sciences*. 461.2055. 609-627.

Schulson, E. M., & Fortt, A. L. 2012. Friction of ice on ice. *Journal of Geophysical Research: Solid Earth*, **117**(B12).

Thomason, J.F. & Iverson, N.R., 2008. A laboratory study of particle ploughing and pore-pressure feedback: a velocity-weakening mechanism for soft glacier beds. *Journal of Glaciology*, **54**(184), pp.169-181.

Wang, K., Johnson, C. W., Bennett, K. C., & Johnson, P. A., 2021. Predicting fault slip via transfer learning. *Nature communications*, **12**(1), 1-11. Doi: 10.1038/s41467-021-27553-5

Zoet, L.K., Carpenter, B., Scuderi, M., Alley, R.B., Anandakrishnan, S., Marone, C., Jackson, M., 2013. The effects of entrained debris on the basal sliding stability of a glacier. *Journal of Geophysical Research: Earth Surface*, **118**, 656-666.

Zoet, L.K., & Iverson, N.R., 2016. Rate-weakening drag during glacier sliding. *Journal of Geophysical Research: Earth Surface*, **121**(7), 1206-1217.

Zoet, L.K. & Iverson, N.R., 2018. A healing mechanism for stick-slip of glaciers. *Geology*, **46**(9), pp.807-810.

Zoet, L.K. & Iverson, N.R., 2020. A slip law for glaciers on deformable beds. *Science*, **368**(6486), pp.76-78.

Zoet, L.K., Ikari, M.J., Alley, R.B., Marone, C., Anandakrishnan, S., Carpenter, B.M., & Scuderi, M.M., 2020. Application of constitutive friction laws to glacier seismicity. *Geophysical Research Letters*, **47**(21), e2020GL088964.